Qiu *et al.*
Protection and Control of Modern Power Systems (2023) 8:33
https://doi.org/10.1186/s41601-023-00308-8

Protection and Control of Modern Power Systems

ORIGINAL RESEARCH

Open Access

Two-stage distributionally robust optimization-based coordinated scheduling of integrated energy system with electricity-hydrogen hybrid energy storage

Yibin Qiu[1,2], Qi Li[1*], Yuxuan Ai[1], Weirong Chen[1], Mohamed Benbouzid[3,4], Shukui Liu[5] and Fei Gao[6]

Abstract

A coordinated scheduling model based on two-stage distributionally robust optimization (TSDRO) is proposed for integrated energy systems (IESs) with electricity-hydrogen hybrid energy storage. The scheduling problem of the IES is divided into two stages in the TSDRO-based coordinated scheduling model. The first stage addresses the day-ahead optimal scheduling problem of the IES under deterministic forecasting information, while the second stage uses a distributionally robust optimization method to determine the intraday rescheduling problem under high-order uncertainties, building upon the results of the first stage. The scheduling model also considers collaboration among the electricity, thermal, and gas networks, focusing on economic operation and carbon emissions. The flexibility of these networks and the energy gradient utilization of hydrogen units during operation are also incorporated into the model. To improve computational efficiency, the nonlinear formulations in the TSDRO-based coordinated scheduling model are properly linearized to obtain a Mixed-Integer Linear Programming model. The Column-Constraint Generation (C&CG) algorithm is then employed to decompose the scheduling model into a master problem and subproblems. Through the iterative solution of the master problem and subproblems, an efficient analysis of the coordinated scheduling model is achieved. Finally, the effectiveness of the proposed TSDRO-based coordinated scheduling model is verified through case studies. The simulation results demonstrate that the proposed TSDRO-based coordinated scheduling model can effectively accomplish the optimal scheduling task while considering the uncertainty and flexibility of the system. Compared with traditional methods, the proposed TSDRO-based coordinated scheduling model can better balance conservativeness and robustness.

Keywords Two-stage distributionally robust optimization, Optimal scheduling, Integrated energy systems, Hydrogen, Uncertainty

*Correspondence:
Qi Li
liqi0800@163.com
Full list of author information is available at the end of the article

1 Introduction

As climate change gathers ever-growing attention globally, countries worldwide are actively pursuing measures to mitigate greenhouse gas emissions. Amidst this transition, renewable energy sources, such as wind and solar power, hold significant practical value, given their low-carbon and eco-friendly attributes. Nevertheless, the output of renewable energy is contingent upon natural conditions, and has inherent uncertainties [1–4]. As renewable energy is increasingly integrated with power systems, this characteristic presents significant challenges to the safe operation of power systems. Renewable energy sources, like wind and solar power, also possess strong seasonal and anti-peak regulation features. Hence, exploring optimal scheduling approaches for power systems that include renewable energy sources has immense theoretical and practical significance in tackling these challenges [5–7].

Currently, there are two main approaches for handling uncertain problems, namely Stochastic Programming (SP) and Robust Optimization (RO) [8]. In [9], scenario sampling using the Stochastic Programming (SP) method was employed to address uncertainty in renewable energy generation so as to reduce the impact of inaccurate renewable energy generation forecasts on system operations. In [10], the SP method was used to construct a novel stochastic-interval model for optimal scheduling of multi-mode photovoltaic-assisted charging stations, where the uncertainties from photovoltaic (PV) generation and energy price were considered in the model. In [11], the SP problem was transformed into a deterministic integer linear programming problem based on constraint linearization and scenario generation techniques to achieve optimal scheduling of multi-energy microgrid systems, whereas in [12], the uncertain output of wind power was analyzed using SP methods, and the scheduling of the energy hub was successfully completed in an uncertain environment. Despite the simple computational procedure offered by the SP method, determining the probability distribution of uncertain issues in advance is often impractical in real-world applications. Moreover, such an approach may yield overly optimistic outcomes, as it entails computing the expectation of all the generated scenarios of uncertainty.

In [13], the RO method was used to handle the uncertainty of photovoltaics, and the demand response of electric vehicles in the energy system was analyzed. In [14], a probabilistic weighted RO method was proposed to address the uncertainties in systems, and the optimal scheduling of the microgrid system was investigated based on this algorithm. The study showed that the proposed method could significantly improve the operational robustness of the system. An optimal scheduling study of a power system integrating PV and hydropower based on the RO method was conducted in [15] to address the optimal operation problem with consideration of load uncertainty. The results indicated that the combination of the hydroelectric system and solar power could bring significant benefits to the power system. In [16], a two-stage robust optimization approach was proposed to minimize the actual operating cost of the microgrid system while considering the uncertainty of renewable energy, and the long-term average operating cost under the service constraint was also minimized. While the RO method can address the issue of optimal operation under uncertainty directly, the resultant solutions may exhibit pronounced conservatism. Moreover, the degree of conservatism is heavily reliant on the selection of the set.

The studies on optimal scheduling of systems considering uncertainty mentioned earlier primarily concentrate on single-energy systems. Nevertheless, researchers have recently introduced the concept of integrated energy systems (IESs), which can effectively enhance the consumption capacity of renewable energy. Hydrogen is characterized by low storage costs, clean and pollution-free profiles, and extensive application potential [17, 18]. The use of hydrogen involves the coupling of electricity, thermal energy, and gas. This is highly compatible with the operating mode of IESs [19, 20]. Thus, research has been conducted on the optimal scheduling of IES with hydrogen units. In [20], a novel and practical deviation satisfaction optimization strategy for IES coupled with renewable energy power generation and hydrogen energy storage was proposed, and its effectiveness was verified by simulation. In [21], an electricity-hydrogen hybrid energy storage IES was proposed, and the optimal scheduling strategy of the system in different seasons was studied. In [22], an optimal energy-reserve scheduling model of a wind-PV-hydrogen IES with multi-type energy storage devices was presented. The case study demonstrated that the proposed energy storage model could reduce the overall operation cost while ensuring the safe operation of the system. In [23], IES combining electricity, thermal energy and hydrogen was established, and their optimal scheduling was studied with actual high-altitude meteorological data. The results demonstrated that the hydrogen storage unit could efficiently meet various demands in the high-altitude residential area. Although the above studies explore the optimal scheduling of IES with hydrogen devices, they ignore the flexibility of IES. Accounting for the flexibility of an IES in optimal scheduling can broaden the scope of scheduling strategies, and by fully leveraging this flexibility, the operational performance of IESs can be substantially improved.

Given the above insights, this paper proposes a coordinated scheduling model based on the two-stage

distributionally robust optimization (TSDRO) for an IES with electricity-hydrogen hybrid energy storage. Compared with previous research, this paper makes the following contributions:

(1) A coordinated scheduling model based on TSDRO is proposed to divide the scheduling problem of IES into two stages. The first stage solves the day-ahead optimal scheduling problem of an IES with deterministic forecasting information, while the second stage builds upon the results of the first stage and uses a distributionally robust optimization method to determine the intraday rescheduling problem under high-order uncertainties. The uncertainties considered include the variability of wind and PV power, and electricity, thermal, and gas loads rather than only a single power-side or load-side uncertainty. The coordinated scheduling model based on TSDRO aims to optimize the total objective value corresponding to the decisions of the two stages in the worst-case scenario of parameters in the second stage.
(2) The coordinated operation of electricity, thermal, and gas networks, as well as the flexibility of these networks and the energy gradient utilization of hydrogen units, are analyzed from the perspectives of economy and carbon emissions in the TSDRO-based coordinated scheduling model.
(3) To improve computational efficiency, the nonlinear formulations in the TSDRO-based coordinated scheduling model are linearized by appropriate methods to obtain a Mixed-Integer Linear Programming (MILP) model. Then, the column-constraint generation (C&CG) algorithm is employed to decompose the scheduling model into a master problem and subproblems. Through the iterative solution of the master problem and subproblems, an efficient analysis of the coordinated scheduling model is achieved.

The rest of this paper is organized as follows. Section 2 provides the component modeling of the IES, while Sect. 3 provides a detailed introduction to the TSDRO-based coordinated scheduling model. Section 4 outlines the solution methodology, and Sect. 5 carries out case studies and presents the corresponding test results. Conclusions are drawn in Sect. 6.

2 Component modeling of the IES

2.1 Structure of the IES

The topology structure of the IES with electricity-hydrogen hybrid energy storage described in this paper is shown in Fig. 1. This system is composed of three subnetworks: electricity, thermal, and gas. The electricity network is required to balance DN, WF, PV, ES, EL, PEMFC, and the electricity load. The thermal network is responsible for considering the energy supply and demand relationship among EB, GB, TR, and thermal load, while the gas network needs to balance the energy supply and demand among HS, GB, and gas load. The linkage between the electricity and gas networks involves the blending of hydrogen into the gas network. The electricity and thermal networks are coupled via EB and TR, while the gas and thermal networks are connected via GB. In addition to meeting their own energy supply and demand requirements, the different subsystems must interoperate with each other to enhance the operational performance of the IES.

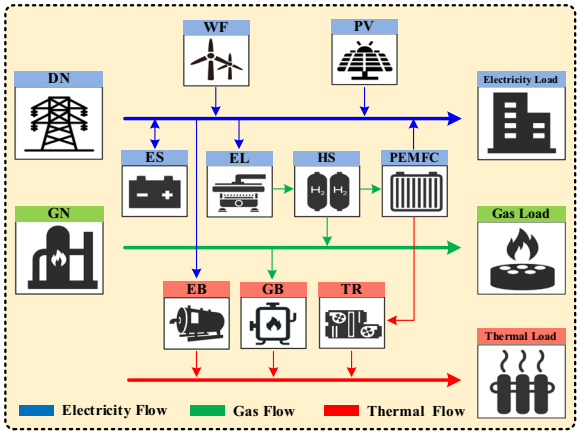

Fig. 1 Topology structure of the IES with electricity-hydrogen hybrid energy storage

2.2 Flexibility component modeling

Currently, IESs have shifted from the previous mode of passive adaptation to load demand towards a coordinated operation between power generation and load. Therefore, this paper specifically incorporates considerations of the flexibilities of electricity, thermal, and gas networks in the optimal scheduling of IES [20, 21, 24]. As for the flexibility of the electricity network, this study mainly focuses on the demand response of the electricity load. The flexibility modeling of demand response units is represented in (1)–(3), where (1) outlines the regulation process of the electrical demand response load, Eq. (2) constrains the magnitude of the demand response regulation, and (3) is designed to ensure that the total load transfer in and out is equal for each operating cycle.

$$\tilde{P}^{t}_{\text{E-DR}} = P^{t}_{\text{E-DR}} + \Delta P^{t}_{\text{E-DR}} \tag{1}$$

$$\Delta P_{\text{E-DR}}^{\min} \le \Delta P_{\text{E-DR}}^{t} \le \Delta P_{\text{E-DR}}^{\max} \tag{2}$$

$$\sum_{t=1}^{N_{\text{T}}} \Delta P_{\text{E-DR}}^{t} = 0 \tag{3}$$

Because of thermal inertia, the temperature does not change abruptly when the thermal energy supply is changed. This allows the thermal network to have a certain degree of flexibility, enabling the consideration of thermal loads as reducible loads that can be reduced during periods of peak demand. Equation (4) describes the flexible regulation process of the thermal load, while (5) limits the magnitude of this flexibility adjustment. Equation (6) provides a constraint on the thermal demand response within the scheduling period. This is used to ensure balance between the increase and decrease of thermal loads during the scheduling period.

$$\tilde{P}_{\text{T-DR}}^{t} = P_{\text{T-DR}}^{t} + \Delta P_{\text{T-DR}}^{t} \tag{4}$$

$$\Delta P_{\text{T-DR}}^{\min} \le \Delta P_{\text{T-DR}}^{t} \le \Delta P_{\text{T-DR}}^{\max} \tag{5}$$

$$\sum_{t=1}^{N_{\text{T}}} \Delta P_{\text{T-DR}}^{t} = 0 \tag{6}$$

As for the flexibility of the gas network, this study mainly considers the flexibility of the hydrogen blending ratio. Research suggests that the impact of hydrogen on the operation of the natural gas network can be neglected when the hydrogen blending ratio is below 10% by volume [25, 26]. Therefore, this paper considers flexible adjustment of the hydrogen blending ratio between 0 and 10% by volume. Based on the assumptions above, Eq. (7) provides the adjustment range of the flexibility of hydrogen blending in the system. As the flexibility of hydrogen blending also involves balance constraints of the gas network, Eqs. (8)–(11) are introduced to represent the corresponding constraints. Specifically, Eqs. (8) and (9) represent the maximum power constraints of the EL and PEMFC, respectively. Equation (10) imposes limits on the State of Hydrogen Charge (SoHC) of the HS at all times, while (11) provides the SoHC consistency constraint.

$$\begin{cases} 0 \le P_{\text{P2G}}^{t} \le \kappa P_{\text{G-Load}}^{t} \\ \kappa = \dfrac{V_{\text{H}_2} E_{\text{H}_2}}{V_{\text{H}_2} E_{\text{H}_2} + (1 - V_{\text{H}_2}) E_{\text{NG}}} \end{cases} \tag{7}$$

$$0 \le P_{\text{EL}}^{t} \le P_{\text{EL}}^{\max} \tag{8}$$

$$0 \le P_{\text{PEMFC}}^{t} \le P_{\text{PEMFC}}^{\max} \tag{9}$$

$$\begin{cases} C_{\text{HS}}^{0} + \left(\eta_{\text{HS}} \sum\limits_{t'=1}^{t} P_{\text{EL}}^{t'} - \dfrac{\sum\limits_{t'=1}^{t} P_{\text{PEMFC}}^{t'}}{\eta_{\text{HS}} \eta_{\text{PEMFC}}^{\text{Ele}}} - \dfrac{\sum\limits_{t'=1}^{t} P_{\text{P2G}}^{t'}}{\eta_{\text{P2G}}} \right) \Delta t \ge C_{\text{HS}}^{\min} \\ C_{\text{HS}}^{0} + \left(\eta_{\text{HS}} \sum\limits_{t'=1}^{t} P_{\text{EL}}^{t'} - \dfrac{\sum\limits_{t'=1}^{t} P_{\text{PEMFC}}^{t'}}{\eta_{\text{HS}} \eta_{\text{PEMFC}}^{\text{Ele}}} - \dfrac{\sum\limits_{t'=1}^{t} P_{\text{P2G}}^{t'}}{\eta_{\text{P2G}}} \right) \Delta t \le C_{\text{HS}}^{\max} \end{cases} \tag{10}$$

$$\eta_{\text{HS}} \sum_{t=1}^{N_{\text{T}}} P_{\text{EL}}^{t} = \frac{\sum\limits_{t=1}^{N_{\text{T}}} P_{\text{PEMFC}}^{t}}{\eta_{\text{HS}} \eta_{\text{PEMFC}}^{\text{Ele}}} + \frac{\sum\limits_{t'=1}^{t} P_{\text{P2G}}^{t'}}{\eta_{\text{P2G}}} \tag{11}$$

2.3 Energy gradient utilization modeling

The working process of PEMFC mainly involves the breaking of H–H and O–O bonds and the formation of H–O bonds. About 60% of the energy released from these reactions is converted into electrical energy, while the rest is dissipated in the form of heat [27]. This study considers using TR for energy gradient utilization for the energy dissipated as heat. The output power constraint of TR during operation and the power calculation method for PEMFC participating in energy gradient utilization are given as:

$$0 \le P_{\text{TR}}^{t} \le P_{\text{TR}}^{\max} \tag{12}$$

$$P_{\text{TR}}^{t} = \min \left(P_{\text{TR}}^{\max}, P_{\text{PEMFC}}^{t} \frac{\eta_{\text{PEMFC}}^{\text{Ther}} \eta_{\text{TR}}}{\eta_{\text{PEMFC}}^{\text{Ele}}} \right) \tag{13}$$

3 TSDRO-based coordinated scheduling model

To achieve optimal scheduling for the IES with electricity-hydrogen hybrid storage, a coordinated scheduling model based on TSDRO is proposed. The objective function and corresponding constraints of the scheduling model are presented in the following sub-sections.

3.1 Objective function

The objective function of the coordinated scheduling model based on TSDRO in this study is calculated as:

$$Obj = \min \left(\underbrace{\sum_{t=1}^{N_{\text{T}}} \left(C_{\text{C}}^{t} + C_{\text{O}}^{t} + C_{\text{M}}^{t} \right)}_{\text{First-stage}} + \underbrace{\max_{\{p_k\} \in \psi} \left(\sum_{t=1}^{N_{\text{T}}} \sum_{k=1}^{K} \left(p_k \min \left(C_{\text{Re\_C}}^{t,k} + C_{\text{Re\_S}}^{t,k} \right) \right) \right)}_{\text{Second-stage}} \right) \tag{14}$$

where

$$C_{\mathrm{C}}^{t}=\alpha_{\mathrm{C}}(\lambda_{\mathrm{DN}}P_{\mathrm{DN}}^{t}+\lambda_{\mathrm{GN}}P_{\mathrm{GN}}^{t})\Delta t \tag{15}$$

$$C_{\mathrm{O}}^{t}=\begin{bmatrix}\rho_{\mathrm{DN}}^{t}P_{\mathrm{DN}}^{t}+\rho_{\mathrm{E\text{-}DR}}\left|\tilde{P}_{\mathrm{E\text{-}DR}}^{t}-P_{\mathrm{E\text{-}DR}}^{t}\right|\\+\rho_{\mathrm{GN}}P_{\mathrm{GN}}^{t}+\rho_{\mathrm{T\text{-}DR}}\left|\tilde{P}_{\mathrm{T\text{-}DR}}^{t}-P_{\mathrm{T\text{-}DR}}^{t}\right|\end{bmatrix}\Delta t \tag{16}$$

$$C_{\mathrm{M}}^{t}=\begin{bmatrix}\alpha_{\mathrm{EL}}P_{\mathrm{EL}}^{t}+\alpha_{\mathrm{PEMFC}}P_{\mathrm{PEMFC}}^{t}+\alpha_{\mathrm{ES}}P_{\mathrm{ES\_ch}}^{t}\\+\alpha_{\mathrm{ES}}P_{\mathrm{ES\_dis}}^{t}+\alpha_{\mathrm{GB}}P_{\mathrm{GB}}^{t}+\alpha_{\mathrm{EB}}P_{\mathrm{EB}}^{t}\end{bmatrix}\Delta t \tag{17}$$

$$C_{\mathrm{Re\_C}}^{t,k}=\begin{bmatrix}\alpha_{\mathrm{C}}(\lambda_{\mathrm{DN}}\tilde{P}_{\mathrm{DN,+}}^{t,s}+\lambda_{\mathrm{GN}}\tilde{P}_{\mathrm{GN,+}}^{t,s})\\-\alpha_{\mathrm{C}}(\lambda_{\mathrm{DN}}\tilde{P}_{\mathrm{DN,-}}^{t,s}+\lambda_{\mathrm{GN}}\tilde{P}_{\mathrm{GN,-}}^{t,s})\end{bmatrix}\Delta t \tag{18}$$

$$C_{\mathrm{Re\_S}}^{t,k}=\begin{bmatrix}\beta_{\mathrm{DN}}^{t}(P_{\mathrm{DN,+}}^{t}+P_{\mathrm{DN,-}}^{t})\\+\beta_{\mathrm{GN}}(P_{\mathrm{GN,+}}^{t}+P_{\mathrm{GN,-}}^{t})\end{bmatrix}\Delta t. \tag{19}$$

As seen, the objective function takes into account the carbon trading cost in (15) and (18), operational cost in (16), maintenance cost in (17), and rescheduling cost in (19) of the IES. Specifically, for day-ahead scheduling, the operational and maintenance costs of the IES are based on deterministic data of PV/WF/electricity load/thermal load/gas load. Because of the uncertainty, this study employs DRO to calculate the intraday rescheduling and carbon trading costs for intraday scheduling [28, 29].

For (16), the calculation of the scheduling cost for the electricity demand response component involves solving for an absolute value and contains nonlinear factors. In order to facilitate subsequent calculations, we introduce auxiliary variables to rewrite this component, as:

$$C_{\mathrm{E\text{-}DR}}^{t}=\beta_{\mathrm{E\text{-}DR}}(P_{\mathrm{E\text{-}DR1}}^{t}+P_{\mathrm{E\text{-}DR2}}^{t})\Delta t \tag{20}$$

$$P_{\mathrm{E\text{-}DR}}^{t}-\tilde{P}_{\mathrm{E\text{-}DR}}^{t}+P_{\mathrm{E\text{-}DR1}}^{t}-P_{\mathrm{E\text{-}DR2}}^{t}=0 \tag{21}$$

$$P_{\mathrm{E\text{-}DR1}}^{t}\geq 0,\ P_{\mathrm{E\text{-}DR2}}^{t}\geq 0. \tag{22}$$

Similarly, the thermal demand response can be expressed as:

$$C_{\mathrm{T\text{-}DR}}^{t}=\beta_{\mathrm{T\text{-}DR}}(P_{\mathrm{T\text{-}DR1}}^{t}+P_{\mathrm{T\text{-}DR2}}^{t})\Delta t \tag{23}$$

$$P_{\mathrm{T\text{-}DR}}^{t}-\tilde{P}_{\mathrm{T\text{-}DR}}^{t}+P_{\mathrm{T\text{-}DR1}}^{t}-P_{\mathrm{T\text{-}DR2}}^{t}=0 \tag{24}$$

$$P_{\mathrm{T\text{-}DR1}}^{t}\geq 0,\ P_{\mathrm{T\text{-}DR2}}^{t}\geq 0. \tag{25}$$

Unlike RO, which constructs the ambitious set directly based on the samples, DRO constructs the ambitious set based on the possible distribution of the samples. Since the actual distribution of the variables is not likely to deviate significantly from the distribution of the samples, the actual distribution can be considered to be included as long as the constraints of the distribution information are reasonable. Thus, only the worst possible distribution situation needs to be found to ensure the result is a lower bound for the performance under the actual sample distribution. By incorporating the distribution information of the samples, the redundant space of the ambitious set can be effectively reduced, thereby decreasing the conservativeness of the RO. The ambitious set of DRO is formulated as:

$$\psi=\left\{p_k\left|\begin{array}{l}p_k\geq 0\\\sum_{k=1}^{K}p_k=1\\\sum_{k=1}^{K}\left|p_k-p_k^0\right|\leq\gamma_1\\\max\left|p_k-p_k^0\right|\leq\gamma_\infty\end{array}\right.,\ k=1,2,\ldots,K\right\}. \tag{26}$$

3.2 Constraints

In order to ensure the proper operation of the IES, some constraints need to be satisfied within and among the subnetworks [30–32]. The constraints of the electricity network were presented in (1)–(3) and are further presented as:

$$0\leq P_{\mathrm{DN}}^{t}\leq P_{\mathrm{DN}}^{\max} \tag{27}$$

$$\begin{cases}0\leq P_{\mathrm{ES\_ch}}^{t}\leq\left(1-U_{\mathrm{ES}}^{t}\right)P_{\mathrm{ES\_ch}}^{\max}\\0\leq P_{\mathrm{ES\_dis}}^{t}\leq U_{\mathrm{ES}}^{t}P_{\mathrm{ES\_dis}}^{\max}\end{cases} \tag{28}$$

$$\begin{cases}C_{\mathrm{ES}}^{0}+\eta_{\mathrm{ES}}\sum_{t'=1}^{t}(P_{\mathrm{ES\_ch}}^{t'}\Delta t)-\frac{\sum_{t'=1}^{t}\left(P_{\mathrm{ES\_dis}}^{t'}\Delta t\right)}{\eta_{\mathrm{ES}}}\geq C_{\mathrm{ES}}^{\min}\\C_{\mathrm{ES}}^{0}+\eta_{\mathrm{ES}}\sum_{t'=1}^{t}(P_{\mathrm{ES\_ch}}^{t'}\Delta t)-\frac{\sum_{t'=1}^{t}\left(P_{\mathrm{ES\_dis}}^{t'}\Delta t\right)}{\eta_{\mathrm{ES}}}\leq C_{\mathrm{ES}}^{\max}\end{cases} \tag{29}$$

$$\eta_{\mathrm{ES}}\sum_{t=1}^{N_{\mathrm{T}}}\left(P_{\mathrm{ES\_ch}}^{t}\Delta t\right)=\sum_{t=1}^{N_{\mathrm{T}}}(P_{\mathrm{ES\_dis}}^{t}\Delta t)\Big/\eta_{\mathrm{ES}} \tag{30}$$

$$\begin{aligned}&P_{\mathrm{DN}}^{t}+P_{\mathrm{ES\_dis}}^{t}+P_{\mathrm{WF}}^{t}+P_{\mathrm{PV}}^{t}+P_{\mathrm{PEMFC}}^{t}\\&=P_{\mathrm{ES\_ch}}^{t}/\eta_{\mathrm{ES}}+P_{\mathrm{EL}}^{t}/\eta_{\mathrm{EL}}+P_{\mathrm{EB}}^{t}/\eta_{\mathrm{EB}}+P_{\mathrm{E\text{-}Load}}^{t}+\tilde{P}_{\mathrm{E\text{-}DR}}^{t}.\end{aligned} \tag{31}$$

Equation (27) is the limit for the IES to purchase electricity from DN. Equation (28) gives the charge/discharge

power limit of ES, while (29) restricts the state of charge (SOC) of ES to satisfy the constraint at all times. Equation (30) ensures the consistency of the first and last SOC of ES, which is a constraint added for continuous scheduling, while (31) guarantees the supply and demand balance of the electricity network.

The constraints of the thermal network were presented in (4)–(6) and (12)–(13), and are further given as:

$$0 \le P_{\mathrm{EB}}^{t} \le P_{\mathrm{EB}}^{\max} \tag{32}$$

$$0 \le P_{\mathrm{GB}}^{t} \le P_{\mathrm{GB}}^{\max} \tag{33}$$

$$P_{\mathrm{GB}}^{t} + P_{\mathrm{EB}}^{t} + P_{\mathrm{TR}}^{t} = P_{\mathrm{T\text{-}Load}}^{t} + \tilde{P}_{\mathrm{T\text{-}DR}}^{t}. \tag{34}$$

Equation (32) represents the operating constraint of the EB. The output power limit of GB is denoted in (33), and (34) limits the equilibrium constraint of the thermal network in terms of energy supply and energy consumption.

The gas network is jointly constrained by (7)–(11) and (35, 36), where (35) gives the limit of IES purchases from GN and (36) is used to constrain the supply and demand balance of the gas network.

$$0 \le P_{\mathrm{GN}}^{t} \le P_{\mathrm{GN}}^{\max} \tag{35}$$

$$P_{\mathrm{GN}}^{t} + P_{\mathrm{P2G}}^{t} = P_{\mathrm{G\text{-}Load}}^{t} + P_{\mathrm{GB}}^{t} / \eta_{\mathrm{GB}} \tag{36}$$

4 Solution methodology

In order to solve the optimization problem mentioned above, the C&CG algorithm is used to decompose the problem into a master-subproblem framework. Specifically, a day-ahead scheduling scheme for the IES is determined in the master problem. In the subproblem, the rescheduling strategy is made to modify the day-ahead scheduling strategy according to the actual situation of generation and load. The optimal scheduling of the IES can be solved in an iterative process [33, 34]. The descriptions of the master and subproblem are introduced below.

First, the master problem aims to find the optimal day-ahead scheduling strategy for the IES based on a known worst-case scenario probability distribution, and the master problem can be expressed as:

$$\begin{cases} \min a^{\mathrm{T}} x + b^{\mathrm{T}} y_0 + W \\ W \ge \sum_{k=1}^{K} p_k^{(m)} (b^{\mathrm{T}} y_k^{(m)}),\ \forall m = 1, 2, \ldots, n \end{cases} \tag{37}$$

Secondly, the subproblem aims to find the worst-case probability distribution situation based on the decision variable x determined by the master problem. The found worst-case probability distribution will be returned to the master problem, which will then determine the optimal scheduling strategy according to the returned worst-case probability distribution to proceed to the next iteration. The specific calculation process of the subproblem is shown as:

$$\max_{\{p_k\} \in \Omega} \sum_{k=1}^{K} p_k \min_{y_k \in Y(x^*, \xi_k)} (b^{\mathrm{T}} y_k). \tag{38}$$

Based on the descriptions of the above objective functions of the master problem and subproblem, the specific solution process of the above TSDRO-based coordinated scheduling model based on the C&CG algorithm is as follows:

Step 1 Initialize the parameters by randomly giving an initial worst-case of the probability distribution, and setting the upper bound of the scheduling cost $UB = +\infty$ and the lower bound $LB = -\infty$. Meanwhile, the iterations counter k is set as 1;

Step 2 Solve the master problem based on the worst probability distribution and obtain the optimal solution x_k of the master problem. Update the lower bound LB with the calculated objective value of the master problem;

Step 3 Solve the subproblem based on x_k, and search for the worst probability distribution within all the constraints mentioned above. Obtain the objective function value of the subproblem $f_k(x_k)$, and update $UB = \min(UB, f_k(x_k))$;

Step 4 If $UB - LB \le \varepsilon$, where ε is a given gap tolerance of C&CG, return the optimal scheduling strategy (x_k, y_k), and then terminate. Otherwise, create variables y_{k+1}, add corresponding constraints in the master problem, update $k = k + 1$ and go to Step2 until the convergence condition of the algorithm is reached.

5 Case study

To verify the effectiveness of the TSDRO-based coordinated scheduling model, it is applied to an IES with a structure similar to that depicted in Fig. 1. The forecasted data associated with the WF and PV, electricity demand response and thermal demand response, as well as electricity, natural gas, and thermal loads, are presented in Fig. 2. These data are predicted based on historical data from a city located in southwestern China. To achieve this objective, the scheduling model for the IES with electricity-hydrogen hybrid energy storage is established using Matlab 2021a on a PC equipped with an Intel(R) Core(TM) i7-1165G7 @ 2.80 GHz. Subsequently, the corresponding scheduling model is analyzed using the Gurobi 10.0 commercial solver [35]. The specific parameters involved in the IES are shown in Table 1 [21, 32, 36–42].

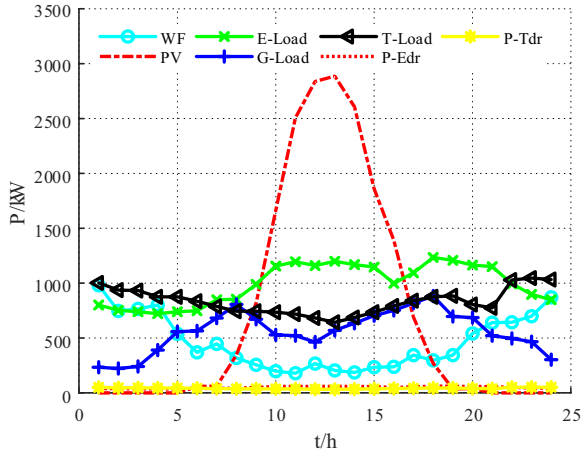

Fig. 2 The forecast output of wind/PV and the forecast load of electricity/gas/thermal/demand response

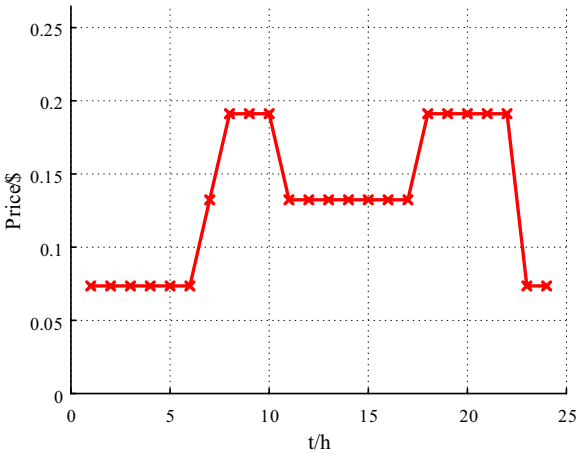

Fig. 3 Price information of the IES with DN

Table 1 The operation parameters of the IES

Devices	Parameters	Value
DN	$P^{max}_{DN\_buy}$/kW	1200
ES	$P^{max}_{ES\_ch}$/kW	200
	$P^{max}_{ES\_dis}$/kW	200
	C^{0}_{ES}/kWh	500
	C^{min}_{ES}/kWh	100
	C^{max}_{ES}/kWh	900
	η_{ES}	0.98
EL	P^{max}_{EL}/kW	1000
	η_{EL}	0.8
HS	C^{0}_{HS}/kWh	5000
	C^{min}_{HS}/kWh	1000
	C^{max}_{HS}/kWh	9000
	η_{HS}	0.95
PEMFC	P^{max}_{PEMFC}/kW	300
	η^{Ele}_{PEMFC}	0.5
	η^{Ther}_{PEMFC}	0.35
GN	$P^{max}_{GN\_buy}$/kW	1200
GB	P^{max}_{GB}/kW	800
	η_{GB}	0.96
EB	P^{max}_{EB}/kW	1000
	η_{EB}	0.938

In this study, the trading price of the IES with GN is set to a constant of 0.1361$/kWh [36, 37]. The step tariff is chosen as the trading price of the DN. The detailed price information of the IES with DN is shown in Fig. 3 [33].

5.1 Convergence results of the C&CG algorithm

When analyzing the TSDRO-based coordinated scheduling model using the C&CG algorithm, an important criterion for determining the success of the solution is whether the upper and lower bounds converge within the specified threshold during the iterative process. To verify the effectiveness of the C&CG algorithm, the iterative process of the upper and lower bounds is analyzed and the results are shown in Fig. 4.

From Fig. 4, it can be observed that in the iterative solving process of the C&CG algorithm, the upper bound of the problem gradually decreases while the lower bound gradually increases. After 20 iterations, the difference between the upper and lower bounds becomes less than 10^{-6}, indicating the completion of the scheduling model based on the C&CG algorithm. This result demonstrates the effectiveness of the C&CG algorithm in analyzing the TSDRO-based coordinated scheduling model.

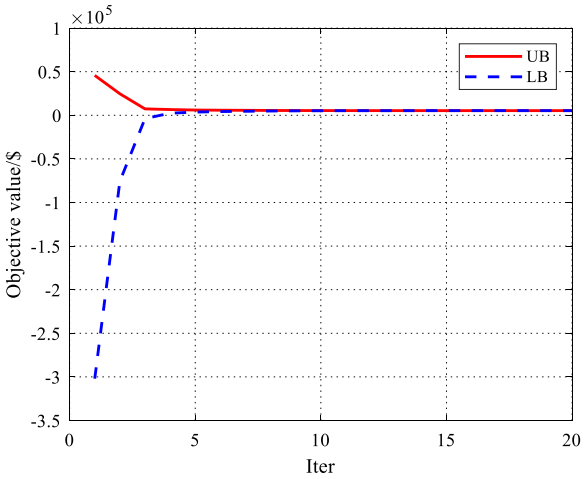

Fig. 4 Iterative process of the C&CG algorithm

5.2 Day-ahead scheduling results

In order to explore the operation of the IES based on the TSDRO-based coordinated scheduling model, the electricity, thermal and gas networks are analyzed from the perspective of energy supply and demand balance using day-ahead scheduling as an example. The operations of the three networks are shown in Fig. 5.

From Fig. 5a, it can be seen that based on the TSDRO-based coordinated scheduling model, the electricity network achieves a supply–demand balance at all scheduling moments. The operational schedule of EL primarily focuses on periods of surplus PV, while FC is mainly operational during high electricity price periods to reduce the purchasing cost of the electricity network. The energy storage of ES is primarily concentrated during low electricity price periods and periods of surplus renewable energy generation, while the discharge process is mainly focused on high electricity price periods.

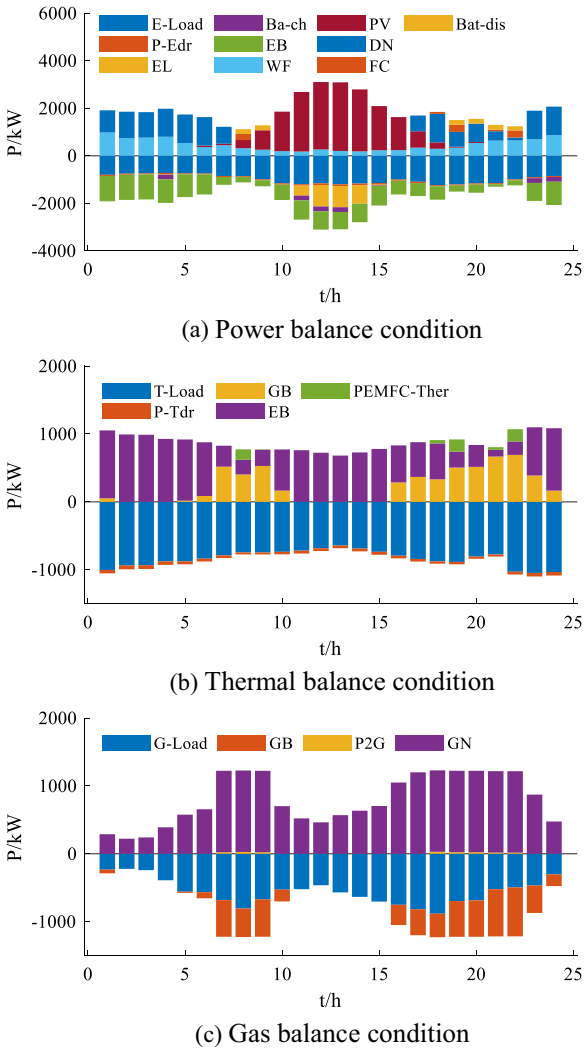

Fig. 5 Energy balance conditions for the IES with electricity-hydrogen hybrid energy storage: **a** electricity network; **b** thermal network; **c** gas network

As illustrated in Fig. 5b, the energy supply and demand of the thermal network have also reached equilibrium. Specifically, the provision of thermal energy mainly relies on GB and EB. Because of the step tariff, the provision of thermal energy in the thermal network primarily depends on EB during low electricity price periods. Moreover, when there is abundant PV during the midday period, there is also a clear tendency to rely on EB for thermal energy provision. TR provides thermal energy during the two high electricity price periods. This is because FC tends to provide electricity during these periods, so TR can only recover waste heat from PEMFC.

From Fig. 5c, it can be seen that the overall supply and demand balance of the gas network within the IES has also been achieved. The energy supply of the gas network is mainly dependent on GN, whereas the proportion of blending hydrogen is only a small fraction. Moreover, hydrogen blending mainly occurs during periods of high electricity prices.

5.3 Analysis of the role of flexibility

This section presents a detailed analysis of the flexible components within the IES to investigate the impact of flexibility on the operational results. A comparison is then made with the IES where flexibility is not considered, so as to emphasize the importance of flexibility in the operation. The scheduling results of the electricity and thermal demand responses are shown in Fig. 6.

From Fig. 6a, it can be seen that the electricity demand response during peak price periods is appropriately reduced after optimization by the TSDRO-based coordinated scheduling model. During valley price periods and in the midday when PV is abundant, the electricity demand response is increased to some extent. Such scheduling results can contribute to reducing operational costs. The results indicate that the electricity demand response, as an important manifestation of flexibility in the IES electricity network, can achieve the goal of reducing IES operating costs by changing the distribution of its own power load.

The findings depicted in Fig. 6b illustrate that the thermal demand response undergoes a scheduling process similar to that of the electricity demand response because of the stepped electricity price. During the two peak price periods of stepped electricity price, the thermal demand response is curtailed. During valley price periods and the midday period with ample PV, it is appropriately increased to ensure the overall level of thermal demand response remains constant within the scheduling period.

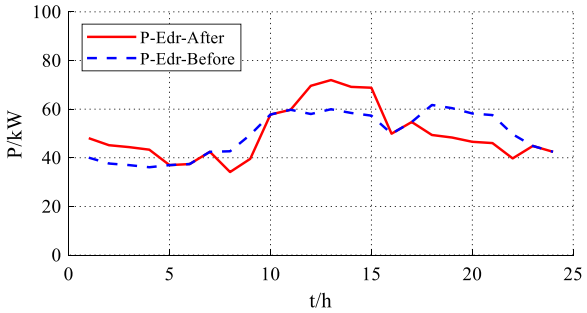

(a) Electricity demand response

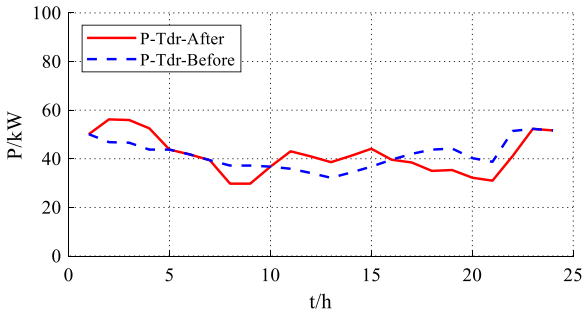

(b) Thermal demand response

Fig. 6 Scheduling results for demand response as flexible components: **a** Electricity demand response; **b** Thermal demand response

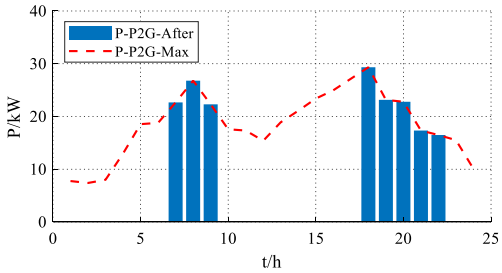

(a) Hydrogen blending

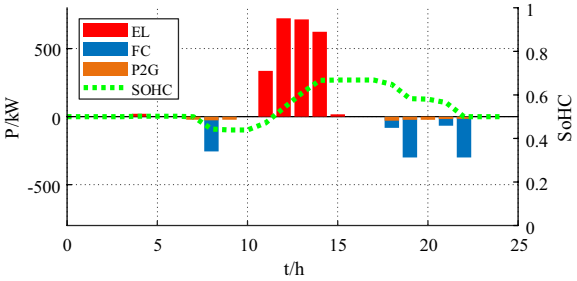

(b) Hydrogen units

Fig.7 Scheduling results of: **a** Hydrogen blending; **b** Hydrogen units

These outcomes demonstrate that the thermal demand response, as a critical flexibility component of the thermal network, can also reduce IES operating costs by changing the distribution of its own thermal load under the TSDRO-based coordinated scheduling model.

As for the flexibility of the hydrogen blending ratio, the hydrogen blending process and the operation of hydrogen units are investigated, and the specific results are shown in Fig. 7.

From Fig. 7a, it can be seen that when the flexibility of the hydrogen blending ratio is considered, hydrogen is not blended into the gas network in the maximum ratio at any time. The hydrogen blending process mainly occurs during peak price periods of the day and is blended at the highest proportion. Because of the step tariff, the IES reduces the use of electricity during peak price periods and consumes gas to provide energy for the power load. When the output power of GN reaches the power limit, the IES increases the blending of hydrogen to continue supplying energy to the power grid, thus reducing operating costs.

For the operational situation of the hydrogen unit considering hydrogen blending flexibility, as demonstrated in Fig. 7b, it can be seen that EL primarily operates during the midday period when renewable energy output is abundant and during valley price periods throughout the day. PEMFC operates during peak price periods, while hydrogen blending also occurs during this time frame. Notably, the SoHC consistently remains within the prescribed constraint range, and returns to the initial state at the end of the daily scheduling.

To further analyze the role of flexibility, optimal scheduling research on the IES is conducted in five different scenarios:

- Scenario 1: IES without considering flexibility;
- Scenario 2: IES considering the flexibility of the electricity, thermal, and gas networks;
- Scenario 3, IES considering only the flexibility of the electricity network;
- Scenario 4, IES considering only the flexibility of the thermal network;
- Scenario 5, IES considering only the flexibility of hydrogen blending.

The specific results are presented in Table 2, with the following main observations:

- When the flexibility of the electricity, thermal, and gas networks is not considered, the carbon trading cost, operational cost, and maintenance cost of the IES are \$806.36, \$4,068.70, and \$599.97, respectively, with a total cost of \$5,475.03.

Table 2 Results comparison of different scenarios

	Carbon trading cost ($)	Operational cost ($)	Maintenance cost ($)	Total cost ($)
Scenario 1	806.36	4068.70	599.97	5475.03
Scenario 2	802.58	4062.94	597.33	5462.85
Scenario 3	806.14	4064.85	599.65	5470.64
Scenario 4	806.17	4065.31	599.69	5471.18
Scenario 5	802.98	4070.17	597.93	5471.07

- When the flexibility of these networks is considered, the corresponding costs become $802.58, $4,062.94, and $597.33, respectively, with a total cost of $5,462.85. It can be seen that considering flexibility can significantly reduce the various costs of the IES.
- When only the flexibility of the electricity network is considered, the corresponding costs become $806.14, $4,064.85, and $599.65, with a total cost of $5,470.64. This is because the electricity demand response is shifted to valley price periods, reducing the cost of purchasing electricity during peak price periods.
- When the flexibility of the thermal network is considered, the corresponding costs become $806.17, $4,065.31, and $599.69, with a total cost of $5,471.18. This is because the thermal demand response is shifted to valley price periods, reducing the cost of purchasing energy.
- When the flexibility of the hydrogen blending is considered, the corresponding costs become $802.98, $4,070.17, and $597.93, totaling $5,471.07. It can be seen that when the hydrogen blending ratio is not fixed, the IES can flexibly adjust the blending ratio to achieve better performance.

These results indicate that considering flexibility in the optimal scheduling of the IES can improve the economic operation of the system. It also further validates that the TSDRO model can effectively handle the IES flexibility.

5.4 Analysis of the role of uncertainty

This study further analyzes the influence of uncertainty on IES optimal scheduling and explores the superiority of the TSDRO-based coordination scheduling model in solving uncertainty problems. Specifically, based on the forecast information on both the IES power supply and demand, 1000 random scenarios are generated according to the numerical characteristics of the historical data prediction error. Then, based on the forecast information and random scenarios, the IES optimal scheduling is studied with the minimum cost of day-ahead scheduling and intra-day rescheduling as the objectives, based on four scenarios:

- Scenario 1: without considering uncertainty;
- Scenario 2: SP-based uncertainty consideration;
- Scenario 3: RO-based uncertainty consideration;
- Scenario 4: TSDRO-based uncertainty consideration.

The results are shown in Table 3. As shown, the scheduling cost of Scenario 1 in the day-ahead stage is $5,394.62, which is lower than the day-ahead scheduling costs of the other three scenarios that consider uncertainty. This is because, after considering the uncertainty, the formulation of the day-ahead scheduling strategy needs to take into account the intra-day rescheduling costs caused by the uncertainty. Given that intra-day rescheduling generally incurs higher costs, the intra-day rescheduling cost of the unit power is generally higher than that of the day-ahead scheduling stage. After considering both day-ahead and intra-day rescheduling processes, Scenarios 2, 3, and 4 adopt more conservative strategies in the day-ahead stage. This is the reason why the day-ahead scheduling costs of the IES with uncertainty are higher than those without uncertainty. However, from the perspective of intra-day rescheduling, Scenario 1 has an average intra-day rescheduling cost of $1,461.99 and a maximum cost of $3,035.25. These are significantly higher than the intra-day rescheduling costs of the other three scenarios. By considering both day-ahead and intra-day rescheduling processes, it can be found that Scenario 1 corresponds to the highest total cost. In extreme scenarios, the scheduling strategy of Scenario 1 incurs the highest cost to maintain the normal operation of the IES. The results effectively demonstrate the importance of considering uncertainty in the scheduling process.

By comparing the scheduling results of Scenarios 2, 3, and 4 in Table 3, it can be seen that the day-ahead scheduling cost obtained by the SP model, which processes uncertainty, is $5436.55 and is the lowest among the three IES optimal scheduling models that consider uncertainty. Furthermore, in the intraday rescheduling stage, its average rescheduling cost is $1257.59, which is also the lowest among the three methods. However, when dealing with extreme scenarios, the scheduling

Table 3 Results comparison of different scenarios

	Day-ahead scheduling cost ($)	Intra-day rescheduling cost ($)	
		Average	Maximum
Scenario 1	5394.62	1461.99	3035.25
Scenario 2	5436.55	1257.59	2962.66
Scenario 3	5518.71	1294.32	2707.16
Scenario 4	5462.85	1278.08	2765.14

strategy based on the SP model corresponds to the highest rescheduling cost among the three methods, reaching $2962.66. The results show that the SP model mainly starts from the average angle of uncertain factors when processing uncertainty and cannot adequately handle uncertainty in extreme scenarios.

The day-ahead scheduling cost obtained by the RO model is $5518.71 and its average intraday rescheduling cost is $1294.32. These are the largest among the three scheduling models considering uncertainty. However, in extreme scenarios, its intraday rescheduling cost is $2707.16, being the lowest among the three models. This indicates that the RO model can effectively consider the worst-case scenarios of IES operation when formulating scheduling strategies. The computational results of the RO-based scheduling model show that its advantage is in handling extreme uncertainty, and its robustness is good. However, its drawback is that the formulated strategy is more conservative, resulting in the highest average intraday rescheduling cost.

The day-ahead scheduling cost, intraday scheduling cost, and extreme value of the TSDRO-based coordinated scheduling model are $5462.85, $1278.08, and $2765.14, respectively, all of which are intermediate values among the three models. The results show that the TSDRO model can effectively balance robustness and conservatism when dealing with uncertain problems, and its superiority is further verified.

5.5 Analysis of the role of hydrogen

To investigate the role of hydrogen in the optimal scheduling of the IES, two further scenarios are considered, i.e., Scenario 1: IES without hydrogen units; and Scenario 2: IES with hydrogen units. Based on these scenarios, the impact of hydrogen on the energy purchase costs from DN/GN and renewable energy consumption of the IES, as well as carbon trading costs are analyzed and the results are presented in Table 4.

As seen from Table 4, the IES without hydrogen units has a carbon trading cost of $856.83, an operational cost of $4397.81, a maintenance cost of $534.21, and a total cost of $5788.85. However, with the introduction of the hydrogen units, the corresponding costs are decreased to $802.58, $4062.94, $597.33, and $5462.85, respectively. These changes are due to the introduction of hydrogen units, which can convert previously unabsorbed renewable energy into hydrogen through EL. Hydrogen can then satisfy the demand for loads in different ways under scheduling, reducing the energy purchasing cost of the IES from DN and GN. In addition, the use of hydrogen as an energy supply does not produce carbon emissions, which further reduces carbon trading costs.

Table 4 Cost comparison of IES in different scenarios

	Carbon trading cost ($)	Operational cost ($)	Maintenance cost ($)	Total cost ($)
Scenario 1	856.83	4397.81	534.21	5788.85
Scenario 2	802.58	4062.94	597.33	5462.85

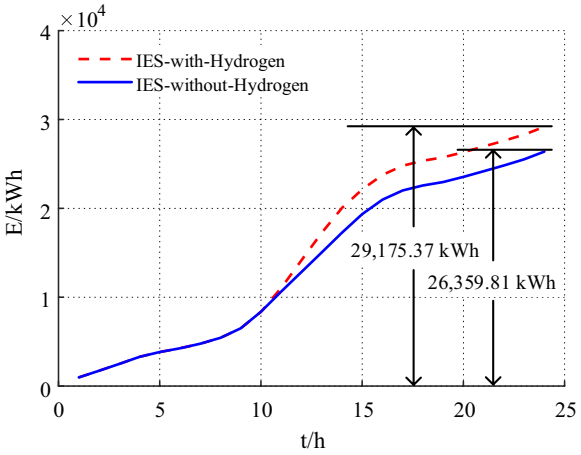

Fig. 8 Comparison of renewable energy consumptions in the IES under different scenarios

For a typical day, the cumulative consumptions of renewable energy in the IES with and without hydrogen units are shown in Fig. 8.

From Fig. 8, it can be seen that during the time period from 01:00 to 10:00, the cumulative renewable energy consumption of the IES with and without hydrogen units overlap, indicating that both types of IES can consume 100% of the renewable energy generated during this period. However, starting from 10:00, the cumulative renewable energy consumption of the IES without hydrogen units begins to deviate from that of the IES with hydrogen units. The deviation trend gradually increases from 10:00 to 17:00 and stabilizes at around 17:00, meaning that during this time period, there are many abandoned WF and PV in the IES without hydrogen units. After 17:00, both types of IES once again consume 100% of the renewable energy generated. By analyzing the data for the entire day, it shows that the IES with hydrogen units consumes 29,175.40 kWh of renewable energy, which is significantly higher than the 26,359.81 kWh for the IES without hydrogen units. These results indicate that the addition of hydrogen units can effectively enhance renewable energy consumption.

6 Conclusions

In this study, a TSDRO-based coordinated scheduling model for IES with electricity-hydrogen hybrid energy storage is proposed. The proposed scheduling model considers the high-order uncertainty and flexibility of the IES, the coordination scheduling among different networks, and the energy gradient utilization of the system. After linearization, the TSDRO-based coordinated scheduling model is analyzed using the C&CG algorithm. Numerical case studies are conducted to verify the effectiveness of the proposed model. Based on the simulation results, it can be concluded that:

(1) The proposed TSDRO-based coordinated scheduling model can effectively achieve the optimal scheduling task while considering the high-order uncertainty of the IES. Compared with traditional methods, the proposed scheduling model can better balance conservativeness and robustness.
(2) The TSDRO-based coordinated scheduling model can effectively coordinate the operation of the electricity, thermal, and gas networks, so as to fully mobilize the flexibility of the IES to achieve better operational performance.
(3) The introduction of hydrogen units can effectively reduce energy purchase costs from DN and GN. Moreover, it can also reduce carbon trading costs and promote renewable energy consumption.

As the current research mainly focuses on small-scale IES, it lacks consideration of the dynamic characteristics of the thermal and gas networks, which is the main limitation of this study. In future work, the dynamic characteristics of thermal and gas networks during scheduling can be further investigated. In addition, because hydrogen and natural gas have different physical properties, the detailed model of the hydrogen blending process also requires further research.

Abbreviations

TSDRO	Two-stage distributionally robust optimization
IES	Integrated energy system
MILP	Mixed-integer linear programming
C&CG	Column-constraint generation
SP	Stochastic programming
RO	Robust optimization
DN	Distribution network
GN	Gas network
WF	Wind farm
PV	Photovoltaic
ES	Energy storage
EL	Electrolyzer
HS	Hydrogen storage tank
PEMFC	Proton exchange membrane fuel cell
GB	Gas boiler
EB	Electric boiler
TR	Thermal recovery

List of symbols

$P^t_{\text{E-DR}}, \tilde{P}^t_{\text{E-DR}}$	Output of power demand response before/after optimization
$\Delta P^t_{\text{E-DR}}, \Delta P^{\max/\min}_{\text{E-DR}}$	Adjustment amount and limits
$P^t_{\text{T-DR}}, \tilde{P}^t_{\text{T-DR}}$	Output of thermal demand response before/after optimization
$\Delta P^t_{\text{T-DR}}, \Delta P^{\max/\min}_{\text{T-DR}}$	Adjustment amount and limits
P^t_{P2G}	Power of hydrogen blending
$P^t_{\text{G-load}}$	Gas load at time t
V_{H_2}	Hydrogen blending ratio in volume
E_{H_2}, E_{NG}	Calorific value of hydrogen and natural gas
$P^t_{\text{EL}}, P^{\max}_{\text{EL}}$	Output of EL and limits
$P^t_{\text{PEMFC}}\ P^{\max}_{\text{PEMFC}}$	Output of PEMFC and limits
$\eta_{\text{ES/HS/P2G/TR/GB/EB}}$	Efficiency of ES, HS, P2G, TR, GB, and EB
$\eta^{\text{Ele/Ther}}_{\text{PEMFC}}$	Electrical/thermal efficiency of PEMFC
$C^0_{\text{HS}}, C^{\max/\min}_{\text{HS}}$	Initial state and capacity limits of HS
$P^t_{\text{TR}}, P^{\max}_{\text{TR}}$	Output of TR and limits
$C^t_{\text{C/O/M}}$	Cost of carbon trading, operation, and maintenance
p_k, p^0_k	The occurrence probability of scenario k
γ_1, γ_∞	L1 norm and infinity norm parameters
$C^{t,k}_{\text{Re\_C/Re\_S}}$	Cost of carbon trading, rescheduling in stage two
$\alpha_{\text{C}}, \lambda_{\text{DN/GN}}$	Cost of carbon processing and carbon emission coefficients for DN/GN
$\rho^t_{\text{DN}}, \rho_{\text{GN}}, \rho_{\text{E-DR/T-DR}}$	Operating prices of DN, GN, E-DR, and T-DR
$P^t_{\text{DN/GN}}, P^{\max}_{\text{DN/GN}}$	Output of DN/GN and its limits
$\alpha_{\text{EL/PEMFC/ES/GB/EB}}$	Cost coefficients of EL, PEMFC, ES, GB, and EB
$P^t_{\text{ES\_ch/ES\_dis}}$	Charge/discharge power of ES
$P^t_{\text{EB/GB}}$	Output of EB and GB
$\tilde{P}^{t,s}_{\text{DN/GN},+}, P^t_{\text{DN/GN},-}$	Adjustment power of DN/GN for upward and downward
$\beta^t_{\text{DN}}, \beta_{\text{GN}}$	Intraday adjustment price of DN/GN
$\beta_{\text{E-DR}}, P^t_{\text{E-DR1/E-DR2}}$	Scheduling price of electricity demand response and its auxiliary variables
$\beta_{\text{T-DR}}, P^t_{\text{T-DR1/T-DR2}}$	Scheduling price of thermal demand response and its auxiliary variables
U^t_{ES}	Status variables of ES
$C^0_{\text{ES}}, C^{\max/\min}_{\text{ES}}$	Initial state and capacity limits of ES
$P^t_{\text{WF}}, P^t_{\text{PV}}$	Output of WF and PV
$P^t_{\text{EB}}, P^{\max}_{\text{EB}}$	Output of EB and its limits
$P^t_{\text{GB}}, P^{\max}_{\text{GB}}$	Output of GB and its limits
$P^t_{\text{E-load}}, P^t_{\text{T-load}}$	Electricity and thermal load at time t

Acknowledgements

We thank the editors and the reviewers for their useful feedback that improved this paper.

Author contributions

YQ was responsible for the methodology, software, validation, formal analysis, and writing the original draft. QL was in charge of formal analysis, visualization, writing the original draft, and reviewing and editing. YA was responsible for software and editing. WC was in charge of resources, review, and editing. Mohamed Benbouzid was responsible for the software, validation, and supervision. SL was in charge of editing and formal analysis. FG was in charge of the software, validation, and supervision. All authors read and approved the final manuscript.

Funding

This work was supported in part by the National Natural Science Foundation (51977181, 52077180), Natural Science Foundation of Sichuan Province (2022NSFSC0027), Fok Ying-Tong Education Foundation of China (171104), 14th Five-year Major Science and Technology Research Project of CRRC (2021CXZ021-2), and Key research and development project of China National Railway Group Co., Ltd (N2022J016-B).

Availability of data and materials

All data generated or analyzed during this study are included in this published article.

Declarations

Competing interests

The authors declare that they have no competing interests.

Author details

[1]School of Electrical Engineering, Southwest Jiaotong University, Chengdu 610031, China. [2]Institut National des Sciences Appliquées de Rennes, 35700 Rennes, France. [3]UMR CNRS 6027 IRDL, University of Brest, 29238 Brest, France. [4]Logistics Engineering College, Shanghai Maritime University, Shanghai 201306, China. [5]Chengdu Power Supply Company, State Grid Sichuan Electric Power Company, Chengdu 610000, China. [6]CNRS, Institut FEMTO-ST, Université de Technologie de Belfort-Montbéliard, 90000 Belfort, France.

Received: 12 December 2022 Accepted: 29 June 2023
Published online: 11 July 2023

References

1. Yao, S., Gu, W., Lu, S., Zhou, S., Wu, Z., Pan, G., & He, D. (2021). Dynamic optimal energy flow in the heat and electricity IES. *IEEE Transactions on Sustainable Energy, 12*(1), 179–190.
2. Ma, R., Song, J., Zhang, Y., Zhang, H., & Yuan, M. (2022). Lifetime-optimized energy management strategy for fuel cell unmanned aircraft vehicle hybrid power system. *IEEE Transactions on Industrial Electronics*. https://doi.org/10.1109/TIE.2022.3206687
3. Ming, H., Xia, B., Lee, K.-Y., Adepoju, A., Shakkottai, S., & Xie, L. (2020). Prediction and assessment of demand response potential with coupon incentives in highly renewable power systems. *Protection and Control of Modern Power Systems*. https://doi.org/10.1186/s41601-020-00155-x
4. Fu, C., Lin, J., Song, Y., Li, J., & Song, J. (2020). Optimal operation of an IES incorporated with HCNG distribution networks. *IEEE Transactions on Sustainable Energy, 11*(4), 2141–2151.
5. Liu, S., et al. (2021). Operational optimization of a building-level integrated energy system considering additional potential benefits of energy storage. *Protection and Control of Modern Power Systems*. https://doi.org/10.1186/s41601-021-00184-0
6. Wen, L., & Song, Q. (2023). ELCC-based capacity value estimation of combined wind-storage system using IPSO algorithm. *Energy, 263*, 125784. https://doi.org/10.1016/j.energy.2022.125784
7. Li, Z., Wu, L., Xu, Y., & Zheng, X. (2022). Stochastic-weighted robust optimization based bilayer operation of a multi-energy building microgrid considering practical thermal loads and battery degradation. *IEEE Transactions on Sustainable Energy, 13*(2), 668–682. https://doi.org/10.1109/tste.2021.3126776
8. Xie, R., Wei, W., Li, M., Dong, Z., & Mei, S. (2023). Sizing capacities of renewable generation, transmission, and energy storage for low-carbon power systems: A distributionally robust optimization approach. *Energy, 263*, 125653. https://doi.org/10.1016/j.energy.2022.125653
9. Shuai, H., Fang, J., Ai, X., Tang, Y., Wen, J., & He, H. (2019). Stochastic optimization of economic dispatch for microgrid based on approximate dynamic programming. *IEEE Transactions on Smart Grid, 10*(3), 2440–2452.
10. Tostado-Véliz, M., Kamel, S., Hasanien, H. M., Arévalo, P., Turky, R. A., & Jurado, F. (2022). A stochastic-interval model for optimal scheduling of PV-assisted multi-mode charging stations. *Energy, 253*, 124219. https://doi.org/10.1016/j.energy.2022.124219
11. Li, Z., & Xu, Y. (2019). Temporally-coordinated optimal operation of a multi-energy microgrid under diverse uncertainties. *Applied Energy, 240*, 719–729.
12. Dolatabadi, M., & Mohammadi-ivatloo, B. (2019). Short-term scheduling strategy for wind-based energy hub: A hybrid stochastic/IGDT approach. *IEEE Transactions on Sustainable Energy, 10*(1), 438–448.
13. Qiu, Y., Li, Q., Huang, L., Sun, C., Wang, T., & Chen, W. (2020). Adaptive uncertainty sets-based two-stage robust optimisation for economic dispatch of microgrid with demand response. *IET Renewable Power Generation, 14*(18), 3608–3615. https://doi.org/10.1049/iet-rpg.2020.0138
14. Zhang, C., Xu, Y., & Dong, Z. Y. (2018). Probability-weighted robust optimization for distributed generation planning in microgrids. *IEEE Transactions on Power Systems, 33*(6), 7042–7051.
15. Apostolopoulou, D., De Greve, Z., & McCulloch, M. (2018). Robust optimization for hydroelectric system operation under uncertainty. *IEEE Transactions on Power Systems, 33*(3), 3337–3348.
16. Hu, W., Wang, P., & Gooi, H. B. (2018). Toward optimal energy management of microgrids via robust two-stage optimization. *IEEE Transactions on Smart Grid, 9*(2), 1161–1174.
17. Wang, T., Li, Q., Wang, X., Chen, W., Breaz, E., & Gao, F. (2020). A power allocation method for multistack PEMFC system considering fuel cell performance consistency. *IEEE Transactions on Industry Applications, 56*(5), 5340–5351.
18. Xing, X., Lin, J., Song, Y., Song, J., & Mu, S. (2020). Intermodule management within a large-capacity high-temperature power-to-hydrogen plant. *IEEE Transactions on Energy Conversion, 35*(3), 1432–1442.
19. Qiu, Y., Li, Q., Wang, T., Yin, L., Chen, W., & Liu, H. (2022). Optimal planning of cross-regional hydrogen energy storage systems considering the uncertainty. *Applied Energy, 326*, 119973. https://doi.org/10.1016/j.apenergy.2022.119973
20. Ma, R., Dang, H., Xie, R., Xu, L., & Zhao, D. (2022). Online fault diagnosis for open-cathode PEMFC systems based on output voltage measurements and data-driven method. *IEEE Transactions on Transportation Electrification, 8*(2), 2050–2061. https://doi.org/10.1109/TTE.2021.3114194
21. Pan, G., Gu, W., Lu, Y., Qiu, H., Lu, S., & Yao, S. (2020). Optimal planning for electricity-hydrogen IES considering power to hydrogen and heat and seasonal storage. *IEEE Transactions on Sustainable Energy, 11*(4), 2662–2676.
22. Wu, G., Li, T., Xu, W., Su, Y., & Liu, J. (2023). Chance-constrained energy-reserve co-optimization scheduling of wind-photovoltaic-hydrogen integrated energy systems. *International Journal of Hydrogen Energy, 48*(19), 6892–6905. https://doi.org/10.1016/j.ijhydene.2022.03.084
23. Wu, Q., & Li, C. (2022). Economy-environment-energy benefit analysis for green hydrogen based integrated energy system operation under carbon trading with a robust optimization model. *Journal of Energy Storage, 55*, 105560. https://doi.org/10.1016/j.est.2022.105560
24. Zhou, J., Wu, Y., Zhong, Z., Xu, C., Ke, Y., & Gao, J. (2021). Modeling and configuration optimization of the natural gas-wind-photovoltaic-hydrogen integrated energy system: A novel deviation satisfaction strategy. *Energy Conversion and Management, 243*, 114340.
25. Timmerberg, S., & Kaltschmitt, M. (2019). Hydrogen from renewables: Supply from North Africa to Central Europe as blend in existing pipelines—Potentials and costs. *Applied Energy, 237*, 795–809. https://doi.org/10.1016/j.apenergy.2019.01.030
26. Jayabal, R., et al. (2022). Multi-objective optimization of performance and emission characteristics of a CRDI diesel engine fueled with sapota methyl ester/diesel blends. *Energy, 250*, 123709. https://doi.org/10.1016/j.energy.2022.123709
27. Wang, C., Li, Q., Wang, C., Zhang, Y., & Zhuge, W. (2021). Thermodynamic analysis of a hydrogen fuel cell waste heat recovery system based on a zeotropic organic Rankine cycle. *Energy, 232*, 121038. https://doi.org/10.1016/j.energy.2021.121038
28. Fu, X. (2022). Statistical machine learning model for capacitor planning considering uncertainties in photovoltaic power. *Protection and Control of Modern Power Systems*. https://doi.org/10.1186/s41601-022-00228-z
29. Zhang, X., Ge, S., Liu, H., Zhou, Y., He, X., & Xu, Z. (2023). Distributionally robust optimization for peer-to-peer energy trading considering data-driven ambiguity sets. *Applied Energy, 331*, 120436. https://doi.org/10.1016/j.apenergy.2022.120436
30. Zhang, T., Guo, Y., Li, Y., Li, Y., & Zhang, J. (2021). Optimization scheduling of regional integrated energy systems based on electric-thermal-gas integrated demand response. *Power System Protection and Control, 49*, 52–61. https://doi.org/10.19783/j.cnki.pspc.200167
31. Xiang, Y., Wu, G., Shen, X., Ma, Y., Gou, J., Xu, W., & Liu, J. (2021). Low-carbon economic dispatch of electricity-gas systems. *Energy, 226*, 120267.
32. Gu, W., Wang, J., Lu, S., Luo, Z., & Wu, C. (2017). Optimal operation for IES considering thermal inertia of district heating network and buildings. *Applied Energy, 199*, 234–246.

33. Liu, Y., Guo, L., & Wang, C. (2018). A robust operation-based scheduling optimization for smart distribution networks with multi-microgrids. *Applied Energy, 228*, 130–140.
34. Qiu, H., Long, H., Gu, W., & Pan, G. (2021). Recourse-cost constrained robust optimization for microgrid dispatch with correlated uncertainties. *IEEE Transactions on Industrial Electronics, 68*(3), 2266–2278.
35. Gurobi Optimization LLC. (2022). Gurobi optimizer reference manual. [Online]. Available: https://www.gurobi.com
36. Chinese, D., Orrù, P. F., Meneghetti, A., Cortella, G., Giordano, L., & Benedetti, M. (2022). Symbiotic and optimized energy supply for decarbonizing cheese production: An Italian case study. *Energy, 257*, 124785. https://doi.org/10.1016/j.energy.2022.124785
37. Song, H., Liu, Y., Bian, H., Shen, M., & Lin, X. (2022). Energy, environment, and economic analyses on a novel hydrogen production method by electrified steam methane reforming with renewable energy accommodation. *Energy Conversion and Management, 258*, 115513. https://doi.org/10.1016/j.enconman.2022.115513
38. Li, S., Zhu, J., Chen, Z., & Luo, T. (2021). Double-layer energy management system based on energy sharing cloud for virtual residential microgrid. *Applied Energy, 282*, 116089. https://doi.org/10.1016/j.apenergy.2020.116089
39. Shi, Z., Liang, Y., Li, H., Dou, W., & Qi, Y. (2022). Interval optimal operation of a multi-objective electric-thermal-transportation integrated energy system considering flexibility. *Power System Protection and Control, 50*, 33–42. https://doi.org/10.19783/j.cnki.pspc.220022
40. Zhang, X., Yu, T., Ma, X., & Guo, L. (2022). An efficient multi-agent negotiation algorithm for multi-period photovoltaic array reconfiguration with a hydrogen energy storage system. *Energy Conversion and Management, 256*, 115376. https://doi.org/10.1016/j.enconman.2022.115376
41. Yang, H., Li, M., Jiang, Z., Liu, X., & Guo, Y. (2020). Optimal operation of regional integrated energy system considering demand side electricity heat and natural-gas loads response. *Power System Protection and Control, 48*, 30–37. https://doi.org/10.19783/j.cnki.pspc.190774
42. Men, Y., Liu, X., & Zhang, T. (2022). Performance research and application of the vapor pump boiler equipped with flue gas recirculation system. *Energy Conversion and Management, 254*, 115201. https://doi.org/10.1016/j.enconman.2021.115201